MTLA 50 (2026) 102877

Contents lists available at ScienceDirect

Materialia

journal homepage: www.elsevier.com/locate/mtla

Full Length Article

A systematic study of sample preparation-induced martensitic phase formation in 304 L austenitic stainless steel

Xingshuo Zhang [a], Anish Ranjan [a], Matthew Luebbe [b], Fan Zhang [b], Haiming Wen [a,*]

[a] Department of Materials Science and Engineering, Missouri University of Science and Technology, Rolla, MO, 65409, USA
[b] Materials Measurement Science Division, National Institute of Standards and Technology, Gaithersburg, MD, 20899, USA

ARTICLE INFO

Keywords:
304 Stainless steels
Austenitic steels
Phase transformation
Deformation induced martensite
Sample preparation

ABSTRACT

Routine sample preparation may unintentionally induce martensitic transformation on the surface of metastable 304 L stainless steel, potentially affecting accurate microstructural characterization. This study systematically investigates the effects of common sample preparation methods such as mechanical cutting, electrical discharge machining (EDM), grinding, and polishing on deformation-induced martensitic transformation on the surface of 304 L stainless steel. Using in-house X-ray diffraction (XRD) and synchrotron-based high-energy XRD, we demonstrate that martensitic transformation is confined primarily to the near-surface region and strongly influenced by the interplay between strain rate and temperature. Mechanical cutting promotes α′-martensite formation with increasing strain rates, whereas thermal effects arising from cutting can suppress transformation by elevating surface temperature above the upper temperature limit for deformation-induced martensite formation. Depending on the preparation route, the measured surface α′-martensite fraction varied from nearly undetectable levels to approximately 0.453. EDM introduced approximately 0.137 vol fraction α′-martensite, likely due to local thermal shock and residual stresses within the resolidified layer. Grinding generated substantial surface α′-martensite because of severe plastic deformation, resulting in α′-martensite volume fraction of 0.286 following mechanical cutting and grinding. In contrast, fine and prolonged polishing largely removed the transformed surface layer, reducing the α′-martensite volume fraction to approximately 0.020 and thereby minimizing its influence on microstructural characterization. These findings emphasize the critical role of sample preparation protocols in accurately characterizing metastable stainless steels. The study provides practical guidelines to minimize preparation-induced artifacts, thereby improving reliability in surface-involved characterizations/investigations.

1. Introduction

304 stainless steel (SS) is one of the most widely used structural materials with broad applications in construction, aerospace and nuclear industries due to its excellent mechanical properties, processability, and oxidation and corrosion resistance [1–3]. 304 SS has a face-centered cubic (FCC) γ-austenitic phase. Austenite is a stable phase at high temperature; however, it is thermodynamically metastable below the equilibrium temperature of γ-austenite and α-ferrite [body-centered cubic (BCC) structured], ~691 °C [4]. The austenite is maintained as a metastable phase during quenching from high temperature to room temperature, additionally with the nickel stabilization. During thermal annealing of 304 L at low-to-intermediate temperatures, the metastable austenite phase may be transformed to ferrite, via a diffusion-controlled process, if there are sufficient thermodynamic driving force and kinetics feasibility. In addition, during ionizing irradiation (e.g., neutron [5] and ion irradiation, as well as focused ion beam sample preparation [6]), austenite to ferrite phase transformation may be triggered [4,7]. Such phase transformation is a significant concern, since it will alter the properties of the 304 SS material. For applications of 304 SS in such environments (e.g., elevated temperature and irradiation), it is important to characterize the microstructure after exposure to study phase composition and phase stability/instability. Many common microstructural characterization techniques, such as lab X-ray diffraction (XRD) and electron backscattered diffraction (EBSD), are limited to (near) surface areas/volumes; they also require sample preparation using electrical discharge machining (EDM), mechanical cutting, and/or mechanical polishing.

* Corresponding author.
E-mail address: wenha@mst.edu (H. Wen).

https://doi.org/10.1016/j.mtla.2026.102877
Received 10 April 2026; Accepted 23 August 2026
Available online 2 September 2026

In addition to the austenite to ferrite phase transformation, another common phase transformation in austenitic SS is austenite to martensite transformation [8]. In austenitic SS, martensitic transformation typically occurs during mechanical stress or deformation (athermal). Thermally induced martensite formation during quenching is not practical in austenitic SS, because the martensite start temperature (Ms) can be extremely low in 304 L stainless steel. For example, no thermally induced martensitic transformation was observed at −196 °C [9]. However, certain undercooling under the equilibrium temperature T_0 of austenite and martensite is still required for deformation-induced martensitic transformation (DIMT), as the chemical driving force is still needed, which is proportional to the undercooling [10]. The mechanical energy from deformation provides an additional driving force [4]. Thus, there is an upper temperature limit for DIMT, termed M_d, above which DIMT will not occur [11]; M_d is ~50–75 °C in 304 SS [12,13]. This DIMT is a diffusionless crystal structure transformation [14,15]. During plastic deformation, the original γ-austenite (FCC) phase, which exhibits excellent ductility and toughness, usually transforms locally into [hexagonal close-packed (HCP)] ε-martensite. This phase provides intermediate lattice distortion and serves as a precursor to α′-martensite. The final α′-martensite [body-centered tetragonal (BCT) or near-BCC due to the very low carbon content] phase is much harder and stronger but significantly less ductile. When the stacking fault energy (SFE) is sufficiently high, γ-austenite can directly transform into α′-martensite without passing through the intermediate ε-martensite [16–18].

Research on DIMT in 304 SS has primarily focused on uniaxial tensile testing conditions. The extent of martensitic transformation is generally influenced by the strain rate, applied stress, and deformation temperature [19–22]. In a study on EN 1.4301 (AISI 304) steel [19], Talonen et al. examined the γ → α′-martensite transformation under two tensile strain rates: 3×10^{-4} s^{-1} and 200 s^{-1}. They demonstrated that the dominant influence of high strain rate was adiabatic heating, which significantly inhibited the DIMT. Similar suppression effects due to thermal rise have also been reported in other deformation experiments [23,24]. In contrast to macroscopic plastic deformation such as conventional tensile loading, martensitic transformation during cutting occurs within localized shear bands, which are characterized by high strain rates and transient deformation conditions. As a result, the transformation mechanism and the amount of α′-martensite formed may differ significantly from those observed under macroscopic loading conditions. Despite its potential significance, research on DIMT behavior during cutting remains limited. In a combined modeling and experimental study, Zhang et al. [25] found that during orthogonal cutting of 304 SS on a CNC lathe, a larger cutting depth and lower cutting speed, under otherwise identical conditions, led to a higher volume fraction of martensite. Interestingly, another study reported that under shear-dominated load conditions during turning, the amount of deformation-induced α′-martensite increased with an increasing strain rate [26].

As mentioned above, characterization of phase composition of steels typically requires sample preparation such as cutting, grinding and polishing, which involves mechanical stress/deformation. However, little attention has been given to the fact that the surface preparation process itself can also introduce DIMT, thereby complicating the interpretation of experimental results. Previous studies have revealed that electropolishing, although often considered a less mechanically invasive technique, can still promote the formation of α′-martensite. The extent of this transformation has been shown to increase with electropolishing duration and applied voltage [27]. In contrast, the potential for mechanical surface preparation methods to induce similar or even more pronounced martensitic transformations has not yet been systematically investigated. This represents a significant gap in the existing literature, especially considering that mechanical preparation steps are far more commonly employed in practical metallographic workflows. Therefore, it is crucial to explore how each step in a typical mechanical preparation sequence contributes to the initiation and evolution of DIMT in metastable austenitic SS. Furthermore, EDM, a widely used preparation method characterized by low mechanical deformation but significant thermal input, was incorporated in this study to serve as a comparative condition to conventional mechanical cutting for assessing their distinct effects on martensitic transformation. Through this investigation, a more comprehensive understanding of how sample preparation affects near-surface phase transformation behavior is developed. Lab-based XRD is employed to probe phase transformation near the surface, while synchrotron-based high-energy XRD measurements are used to establish the bulk reference state. The results address a notable gap in the literature and provide practical guidance for the design and interpretation of surface characterization studies involving metastable austenitic steels.

2. Materials and methods

2.1. Raw material

Commercial coarse-grained 304 L SS was selected as the experimental material. The raw material was in the form of a cylindrical bar with a diameter of 20 mm. The specimens were austenitized at 1050 °C for 1 h and then water-quenched to obtain a fully austenitic structure. Disks with a diameter of 20 mm and a thickness of approximately 2 mm were obtained after cutting. The chemical composition [4,28] of the 304 L SS used in this study was determined by chemical analysis performed by Exova Inc., an accredited commercial laboratory, using inductively coupled plasma (ICP), optical emission spectroscopy (OES), combustion, and gravimetric methods. The measured composition is listed in Table 1. The average grain size of the solution-annealed 304 L stainless steel was measured by EBSD to be 15 ± 9 μm.

2.2. Mechanical cutting and EDM cutting

To evaluate the effect of mechanical cutting (hereafter referred to as Mecut) on the martensitic transformation, experiments were designed with feed rates (the distance the tool or workpiece moves in the feed direction per minute) of 6.35 mm (0.25 in)/min under good cooling conditions; cutting speeds (the fixed axis speeds of the alumina saw blade) of 105, 210, 315, 420, and 525 rad/s, corresponding to 1000, 2000, 3000, 4000, and 5000 rpm, respectively; cutting at 315 rad/s (3000 rpm) with feed rates of 2.54, 5.08, 6.35 mm/min, corresponding to 0.1, 0.2 and 0.25 in/min. In addition, to isolate the effect of potential adiabatic heating effects, cutting was executed under good cooling conditions (coolant maintained at room temperature, ~22–25 °C, with continuous flow) and without coolant at a speed of 315 rad/s (3000 rpm) and a feed rate of 6.35 mm/min. Lab XRD characterization was performed directly on the machined surfaces. All Mecut in this study was completed using a TechCut 5x precision high speed saw[1] (Allied High Tech Products, Cerritos, CA) equipped with a resin-bonded alumina abrasive cut-off wheel (Allied High Tech Products, model 80–11,300) with a diameter of 127 mm (5 in.) and a thickness of 0.38 mm (0.015 in.). During coolant-assisted cutting, the coolant was continuously supplied at a flow rate of approximately 3.6 L/min to maintain a flooded cutting condition and facilitate heat removal from the cutting zone.

Wire cutting was carried out using a Hansvedt DS-2 traveling wire EDM system, with a pulse duration of 0.6 μs and a discharge current of 3.0 A. Similarly, lab XRD characterization was conducted directly on the

[1] Certain commercial equipment, instruments, software, or materials are identified in this paper to foster understanding. Such identification does not imply recommendation or endorsement by the Department of Commerce or the National Institute of Standards and Technology, nor does it imply that the materials or equipment identified are necessarily the best available for the purpose.

Table 1
Bulk composition of 304 L stainless steel used in this study (wt.%).

Fe	Cr	Ni	Mn	Cu	Si	Mo	Ti	P	N	C	S
Bal.	17.33	8.97	1.13	0.64	0.37	0.29	0.28	0.033	0.04	0.014	< 0.002

as-cut surface.

2.3. Grinding and polishing

The grinding and polishing steps in this study were completed using a Tegramin-30 automatic polisher (Struers, Cleveland, OH). The force used in the grinding process was 120 N, and water was used as coolant. The force used in the polishing process was 100 N; no coolant was used, and only BlueLube from Allied High Tech Products was used as a polishing lubricant. During the polishing and grinding processes, the rotational speeds of grinding/polishing disc and sample holder were 10 rad/s (100 rpm) and 5 rad/s (50 rpm), respectively, while maintaining the same direction of rotation. In this study, grinding is defined as grinding the sample surface with grit silicon carbide paper (including P180, P400, P1200, P2400, P4000) from Allied High Tech Products, and polishing is defined as polishing the sample surface on an Imperial adhesive back disc with polishing paste or polishing suspension (including 9 μm, 3 μm, 1 μm, 0.1 μm polycrystalline diamond composite polishing paste and 0.05 μm alumina suspension, or 0.02 μm colloidal silica suspension) from Allied High Tech Products. To evaluate the feasibility of eliminating or minimizing α′-martensite "artifacts" introduced during sample preparation, a series of controlled polishing experiments were conducted on mechanically sectioned specimens prepared at a rotational speed of 315 rad /s (3000 rpm) and a feed rate of 5.08 mm/min. The surfaces were subjected to sequential fine polishing with durations ranging from 50 min to 13 h, followed by XRD characterization. Detailed results and analyses are presented in Section 3.3.

2.4. XRD characterization and martensitic volume fraction calculations

XRD measurements were carried out using an X'Pert PRO diffractometer (Malvern Panalytical Ltd, Malvern, UK) equipped with a PIXcel detector and Cu Kα radiation ($\lambda = 1.5418$ Å), operating at 45 kV and 40 mA. Data were collected over a 2θ range of 30°–80°, with a total scan time of 30 min and a step size of 0.026° The specimens were disk-shaped with a diameter of 20 mm and a thickness of ~2 mm. All XRD characterizations were performed on the cut surfaces without any additional treatment of the samples. Background subtraction of the raw XRD data was conducted using Jade 6.0 software. The volume fraction of the α'-martensite phase was estimated based on the analysis of the XRD peak intensities. The specific calculation involved the use of the following equation [29]:

$$I_{(hkl)\alpha} = \frac{I_0 \lambda^3}{64\pi r}\left(\frac{e^2}{m_e c^2}\right)^2 \frac{M_{(hkl)}}{V_\alpha^2}|F_{(hkl)\alpha}|^2 \left(\frac{1+\cos^2(2\theta)\cos^2(2\theta_m)}{\sin^2(\theta)\cos\theta}\right)_{hkl} \frac{v_\alpha}{\mu_s} \quad (1)$$

Here, I_0 is the incident beam intensity, r is the distance from the sample to the detector, λ is the X-ray wavelength, $e^2/m_e c^2$is the classical electron radius,μ_s is the linear attenuation coefficient of the specimen, $M_{(hkl)}$ is the multiplicity of the *hkl* reflection of phase α ferrite, V_α is the unit cell volume of phase α, v_α is the volume fraction of phase α, $2\theta_m$ is the diffraction angle of the monochromator, and $(1+\cos^2(2\theta)\cos^2(2\theta_m)/\sin^2(\theta)\cos\theta)_{hkl}$ accounts for the Lorentz and polarization corrections. Due to the very low carbon content of 304 L SS, BCT martensite is essentially equivalent to BCC ferrite, and thus the volume fraction of α'-martensite can be obtained from the peak intensity ratio of {110} ferrite to {111} austenite.

The reported α′-martensite fractions provide reasonable quantitative estimates of the transformation level. Although XRD phase quantification is subject to inherent uncertainties associated with diffraction-based measurements, all specimens originated from the same solution-annealed and water-quenched material and were analyzed using a consistent procedure. Therefore, the reported phase fractions remain reliable for quantitative comparison of preparation-induced changes, although they should not be interpreted as exact absolute phase fractions.

2.5. High-energy XRD measurements

High-energy XRD (HE-XRD) measurements were performed at Sector 1-ID of the Advanced Photon Source, Argonne National Laboratory. 304 L SS samples were cut to ~2 mm in thickness, with their surfaces prepared following the protocols described in Section 2.3. All HE-XRD characterizations were performed in transmission geometry, with the cut/prepared surface included within the illuminated sample volume. No additional surface treatment was applied prior to measurement. We used a Pilatus 2 M CdTe single-photon counting detector for X-ray detection purpose.

For these measurements, we used X-rays at an energy of 61.332 keV, which, even for a sample thickness of 2 mm, provides a transmission of 24.5% for pure Fe, hence providing the ground truth for the bulk fractions of phases present in the sample. Here, the transmission is defined as the ratio between the intensity of the transmitted direct X-ray beam and the intensity of the incident beam. This transmission allows structural information from the bulk material to be captured. In contrast, as previous work has shown, the penetration depth of Cu Kα in Fe at the diffraction angle corresponding to the FCC {111} peak, the reflection with the highest theoretical intensity, is only 2.4 μm for the lab-based Bragg-Brentano geometry [30]. Hence, in-house Cu Kα based XRD provides structural information near surface.

By combining the in-house XRD measurements that provide surface-sensitive results and the high-energy synchrotron XRD, which probes the bulk structure, we can systematically evaluate the effect of DIMT on the near-surface phase composition.

3. Results and discussion

3.1. Martensitic transformation during mechanical cutting

Fig. 1. shows the effect of cutting speed on the martensitic transformation in 304 L SS at a constant feed rate (6.35 mm/min). As shown in the XRD patterns in Fig. 1(a), as the cutting speed increases from 105 to 525 rad/s (1000 to 5000 rpm), the α′ {110} (corresponding to strain-induced α′-martensite) peak intensity increases significantly, indicating that deformation-induced martensite is formed during the cutting process, and a higher cutting speed results in more α′- martensite formation through DIMT. Fig. 1(b) quantifies the change in volume fraction of the α′ phase with the rotation speed, which shows a nonlinear growth trend. The volume fraction increases sharply in the range of 315 rad/s to 420 rad/s (3000–4000 rpm) (0.149 → 0.317) and then stays approximately the same beyond 420 rad/s (4000 rpm).

This phenomenon may be attributed to the combined effects of strain rate and localized thermal influences. The notable increases in α′-martensite content at cutting speed up to 420 rad/s (4000 rpm) indicate that the influence of strain rate outweighs that of thermal effect. However, beyond this range, the accumulation of heat might increasingly suppress the driving force for α′-martensite nucleation. According to Olson and Cohen [31], martensite nucleation in metastable austenitic steels occurs preferentially at the intersections of shear bands generated during plastic deformation. An increase in cutting speed generally leads

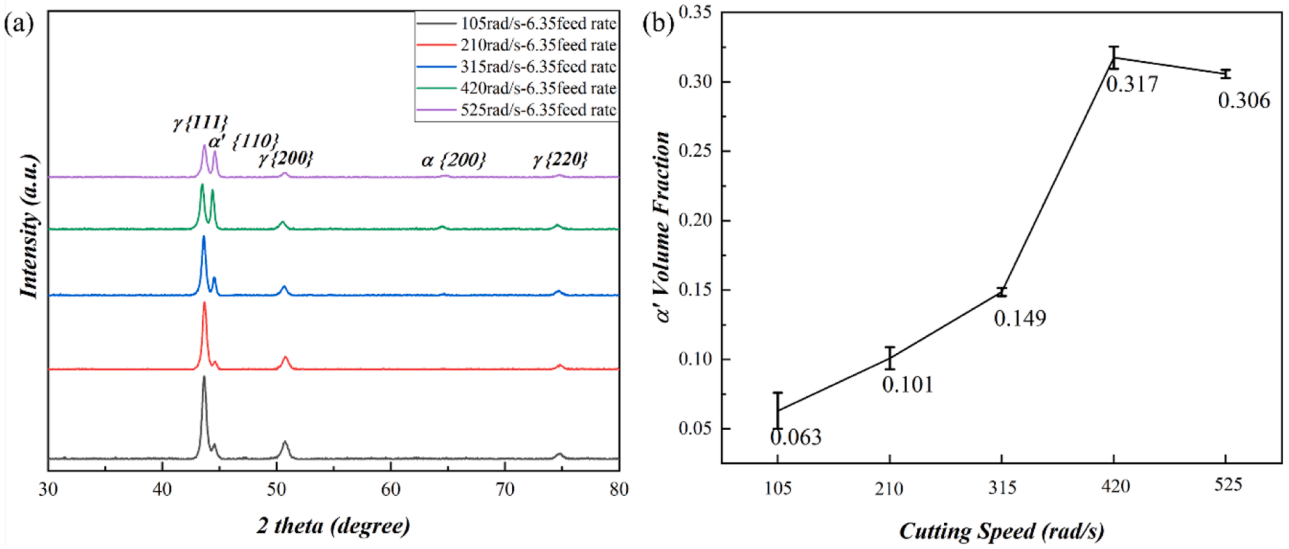

Fig. 1. (a) XRD patterns of the as-cut 304 L SS samples acquired using Cu Kα radiation. The cutting feed rate was kept constant at 6.35 mm/min and the blade cutting speed was varied from 105 rad/s (1000 rpm) to 525 rad/s (5000 rpm), with good cooling. Since all cutting or surface preparation processes inherently introduce DIMT, a true undeformed control sample is not available. The initial state of the material after solution annealing at 1050 °C for 1 h and then water quenched (fully austenitic structure) is used as the reference condition. (b) Corresponding α′-martensite volume fractions under different cutting speeds. The uncertainties shown in this figure represent one standard deviation based on model refinement.

to a higher strain rate [32], which accelerates the formation of shear bands [20] and thereby promotes rapid generation of the α′ phase, while also producing more heat per unit time. Due to the introduction of coolant, the heat generated during cutting is efficiently dissipated at lower cutting speeds (< 420 rad/s, or 4000 rpm), and the adiabatic heating effect is suppressed. At this stage, the α′-martensite phase transformation is mainly controlled by the strain rate. As the strain rate increases, the degree of DIMT on the material surface also increases. A reasonable inference is that, when the cutting speed is high enough (> 420 rad/s, or 4000 rpm), the adiabatic heating effect generated by cutting cannot be offset by the coolant. This may lead to a local temperature rise in the cutting zone, reducing the chemical driving force for martensitic transformation and thereby suppressing DIMT. Cao et al. [33]employed an alternating-current voltage method to measure the relative magnetic permeability, which was then used to determine the martensite volume fraction in 304 SS during tensile deformation. Under high strain rates in impact tensile tests, they observed a similar suppression effect, leading to the similar observations. It should also be noted that grain size may influence deformation-induced martensitic transformation in metastable austenitic stainless steels, with finer grains often reported to enhance austenite stability [34] and suppress martensitic transformation. Since all samples in the present study originated from the same solution-annealed material batch, grain size was not treated as an independent variable.

Fig. 2. displays the XRD patterns of 304 L SS samples cut at different feed rates of 2.54, 5.08, and 6.35 mm/min at a constant rotation speed of 315 rad/s; all cuts were performed under good cooling conditions (indicated by "-G") as described in Section 2.2. The intensity of the α′ {110} peak decreases with increasing feed rate, indicating that lower feed rates promote martensite transformation. While higher feed rates naturally increase strain rates, they also shorten the cooling time, resulting in reduced heat dissipation, especially in the local cutting area. The reduction of α′-martensite observed at higher feed rates under constant cooling suggests that the accumulation of heat exceeds the strain rate effect, increasing the material surface temperature and inhibiting the martensitic phase transformation. These findings further confirm that cooling efficiency plays a crucial role in controlling martensitic transformation.

In order to separate the influence of the thermal effect introduced by

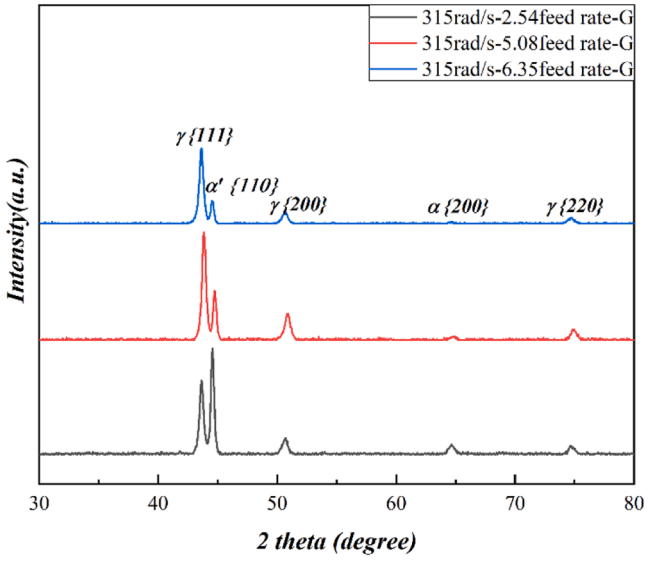

Fig. 2. XRD patterns of as-cut 304 L SS samples collected using Cu Kα radiation. The cutting speed was controlled at 315 rad/s, or 3000 rpm under good cooling conditions, and the cutting feed rate was varied between 2.54 and 6.35 mm/min.

cutting, the samples were cut with and without cooling at a feed rate of 6.35 mm/min and a constant speed of 315 rad/s (3000 rpm) and characterized by lab XRD as shown in Fig. 3. The "-N" in the figure represents no coolant during cutting. It can be observed that in the case without coolant, the DIMT is completely suppressed. The corresponding calculated values of the α′-martensite phase volume fraction in the above discussion is shown in Table 2. At 315 rad/s and under good cooling conditions, as the feed rate increases, the volume fraction of α′-martensite gradually decreases from 0.453 at 2.54 mm/min to 0.149 at 6.35 mm/min. Under no cooling, the volume fraction of α′-martensite is negligible. As temperature increases, the free energy of austenite (γ) decreases faster than that of martensite (α′), which reduces the difference in Gibbs free energy between austenite and α′-martensite and

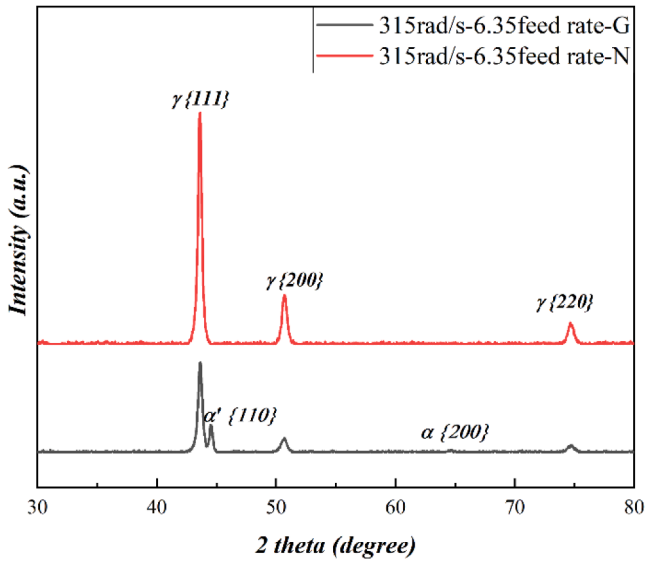

Fig. 3. XRD patterns of as-cut 304 L SS samples collected using Cu Kα radiation. The cutting speed was controlled at 315 rad/s or 3000 rpm, and the cutting feed rate was 6.35 mm/min. Cutting was performed with good cooling (G) and no cooling (N) to isolate the effect of temperature.

Table 2
α′-martensite volume fraction based on XRD under different cutting conditions, with the uncertainties shown representing one standard deviation based on model refinement.

Cutting conditions	α′ martensitic volume fraction
304L-315 rad/s −2.54feed-G	0.453± 0.003
304L-315 rad/s −5.08feed-G	0.210 ± 0.002
304L-315 rad/s −6.35feed-G	0.149 ± 0.002
304L-315 rad/s −6.35feed-N	Not detectable

reduces the chemical driving force for martensitic transformation [35,36], while the SFE increases, thereby inhibiting the occurrence of twinning and phase transformation [37–39]. When the deformation surface temperature is high enough, the martensitic transformation is completely suppressed. This phenomenon supports the hypothesis that local adiabatic heating can raise the surface temperature above the Md temperature, thereby suppressing α′-martensite nucleation. Therefore, for surface-sensitive techniques such as EBSD, strictly controlling the sample preparation temperature (typically requiring it to exceed 50 °C [12]) can effectively prevent the formation of α′-martensite.

3.2. Martensitic transformation during EDM/mechanical cutting and surface finishing

3.2.1. Effect of surface finishing on α′-martensite transformation after EDM and mechanical cutting

Fig. 4 presents the XRD patterns of 304 L SS specimens processed by EDM and Mecut, followed by sequential surface treatments (grinding and polishing). The EDM process was conducted with a pulse duration of 0.6 μs and a peak current of 3 A. The Mecut process was conducted under conditions of relatively low coolant flow rate. The cutting speed was 420 rad/s (4000 rpm), with a feed rate of 5.08 mm/min. As discussed previously, the reduced cooling efficiency led to heat accumulation during cutting, which suppressed the α′-martensitic transformation. Consequently, the α′-martensite phase volume fraction in the as-Mecut sample was limited to 0.084. Quantitative analysis of the α′-martensite phase volume fraction is shown in Table 3. Both EDM and Mecut resulted in γ → α′-martensitic transformation, with α′-martensite volume fractions of 0.137 for EDM and 0.084 for Mecut. Comparison of EDM and Mecut samples leads to an important conclusion: although EDM is nominally free of mechanical stress [40,41], it still leads to significant α′-martensite formation, which may be associated with local thermal shock and residual stresses within the resolidified layer, as suggested in previous studies [41–43]. Additional EDM experiments were performed at peak currents of 5 A and 7 A while maintaining all other processing

Table 3
α′-martensite volume fraction based on XRD of 304 L SS after EDM and mechanical cutting (Mecut) followed by different surface treatments, with the uncertainties shown representing one standard deviation based on model refinement.

Sample preparation conditions	α′ martensitic volume fraction
304L-EDM	0.137± 0.016
304L-EDM+Grind	0.318 ± 0.016
304L-EDM-Grind+Polish	0.199 ± 0.006
304L-Mecut	0.084 ± 0.004
304L-Mecut+Grind	0.286 ± 0.004
304L-Mecut+Grind+Polish	0.204 ± 0.004

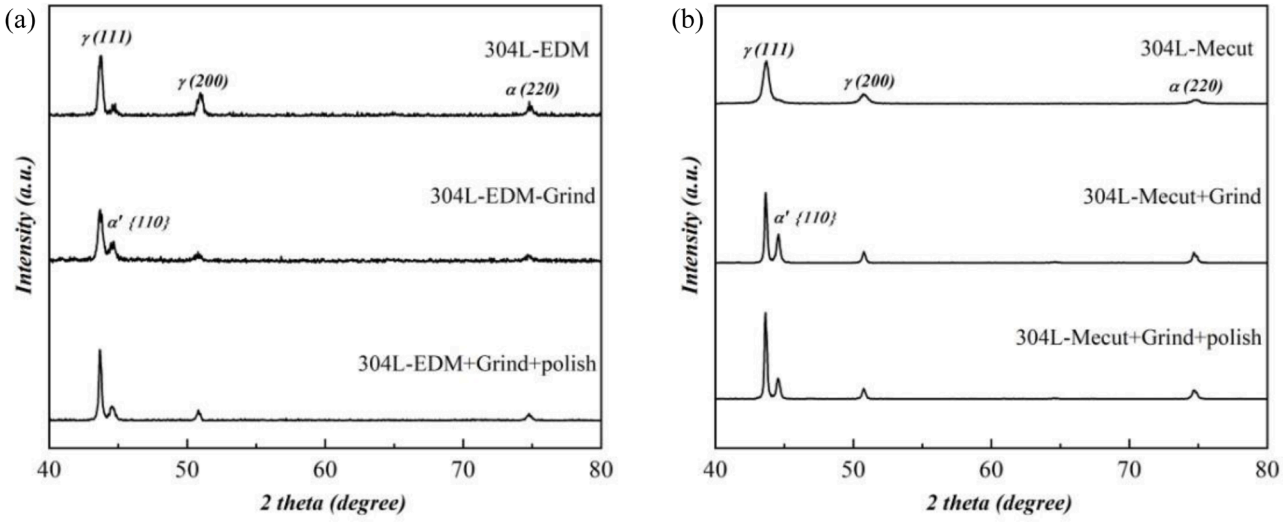

Fig. 4. XRD patterns of as-cut 304 L SS samples collected using Cu Kα radiation: (a) samples processed by EDM, followed by grinding and polishing; (b) samples processed by mechanical cutting (Mecut), followed by grinding and polishing.

parameters. No measurable changes in the XRD patterns associated with α′ martensite were observed among the 3 A, 5 A, and 7 A conditions, suggesting that discharge current had a negligible influence on α′-martensite formation within the investigated parameter range.

After surface grinding (sequentially using silicon carbide abrasive papers of P180, P400, P1200, P2400, and P4000 grit sizes for 1 min, 1 min, 1 min, 1 min, and 2 min, respectively), the α′-martensite volume fraction in both samples were significantly enhanced to 0.318 for EDM and 0.286 for Mecut. This increase is attributed to the fact that this grinding step introduces additional deformation sufficient to further promote the γ → α′ martensitic transformation in the near-surface region. After polishing (sequentially using 9 μm, 3 μm, and 1 μm diamond suspensions for 2 min, 5 min, and 5 min, respectively), the α′-martensite volume fractions decreased to 0.199 for EDM and 0.204 for Mecut. This phenomenon may be attributed to the removal of the most severely deformed surface layer during polishing, which is likely to have reduced the apparent α′-martensite content. In addition, since the martensite contents measured from laboratory XRD for both specimens after polishing were very close, it is also possible that polishing may have removed a large amount of pre-existing surface α′-martensite while simultaneously inducing some degree of new martensitic transformation under the surface.

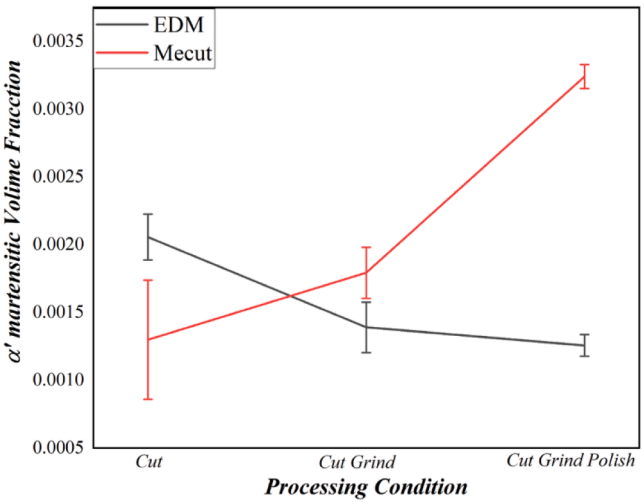

Fig. 6. α′-martensitic phase volume fraction in 304 L SS under various processing conditions (results from high-energy XRD), with the uncertainties shown representing one standard deviation based on model refinement.

3.2.2. *High-energy XRD characterization*

Although a decrease in the volume fraction of α′-martensite was observed after polishing, it is still uncertain whether the polishing process itself causesh new DIMT. In order to investigate the extent and depth of phase transformation under various cutting and surface treatment conditions, HE-XRD was used for phase composition analysis, and the results are shown in Fig. 5. From the close-up view of the α′-martensite peak (Fig. 5. b), α′-martensite was present in different samples. However, the α′-martensite peak is extremely weak in all the samples, suggesting that the content of bulk α′-martensite phase under different processing conditions was basically the same. This result indicates that from the perspective of bulk samples, the DIMT introduced by EDM, Mecut, grinding and polishing is very limited and confined to the near-surface region probed by in-house XRD measurements.

Fig. 6. Further illustrates this point based on the quantitative volume fraction of α′-martensite measured by HE-XRD. The α′-martensite volume fraction in all samples is <0.0035, which indicates that the DIMT caused by the above processing process only occurs on the extreme surface [27] of the sample. The volume fraction of α′-martensite in EDM-cut samples decreased after grinding and polishing (from 0.002 to 0.001), while the volume fraction of α′-martensite in Mecut samples increased slightly after grinding and polishing. This is because the bulk material was predominantly austenitic, and the contribution from near-surface deformation-induced α′-martensite to the overall volume fraction was minimal. Due to possible slight variations in the initial sample thickness, no further comparison of trends was attempted. At the same time, this finding also suggests the possibility of removing surface deformation-induced α′-martensite by fine polishing.

To clarify the depth sensitivity of the measurements, it is important to note that lab XRD using Cu Kα radiation provides a penetration depth of ~1–5 μm [44] in austenitic SS, thus mainly reflecting surface structural information. In contrast, HE-XRD (with photon energies above 50–80 keV) can achieve penetration depths of several millimeters [45] enabling the characterization of the bulk structure. This fundamental difference in probing depth explains why HE-XRD detects only a minor amount of α′-martensite, while lab XRD shows a significantly higher surface martensite content.

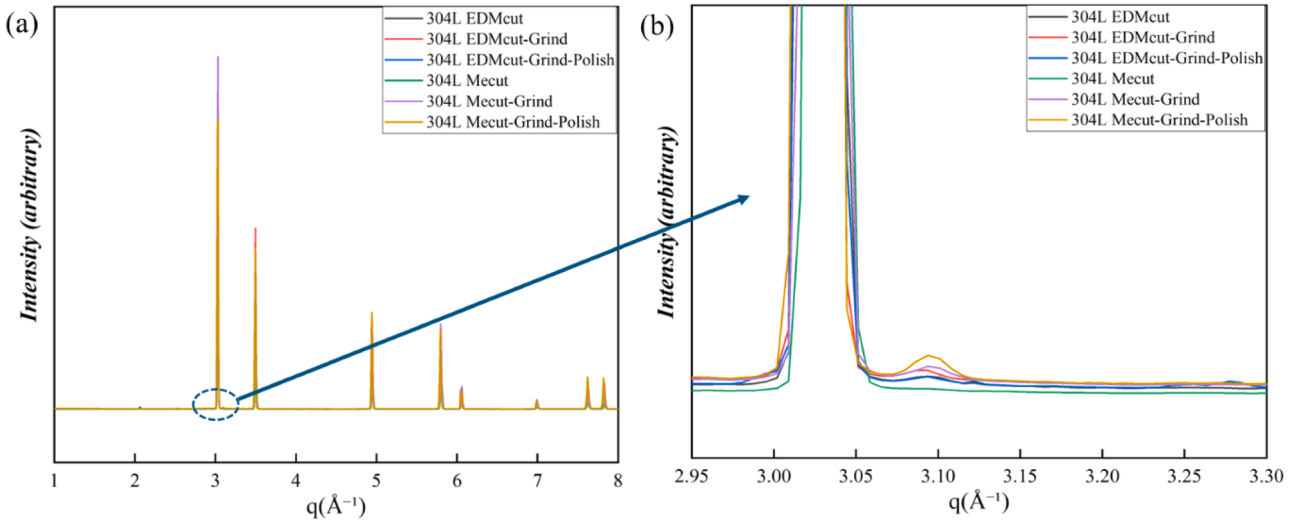

Fig. 5. (a) HE-XRD patterns of 304 L SS after mechanical cutting (Mecut) [the cutting speed of this sample is 420 rad/s (4000 rpm) and the feed rate is 5.08 mm (0.20in) /min] or EDM, followed by grinding and polishing; (b) magnified view of the dashed-line region, showing the presence of α′-martensite.

3.3. Effect of prolonged polishing on surface α′-martensite content

Since martensitic phase transformation primarily occurs within the extreme surface layer during sample preparation, it is crucial to investigate whether prolonged fine polishing can effectively eliminate or minimize the influence of DIMT on characterization results. This task examines the evolution of the α′-martensite volume fraction under varying polishing durations. The lab XRD patterns corresponding to different polishing times are presented in Fig. 7. The quantified α′-martensite volume fractions after different steps are displayed in Table 4. After Mecut, the α′-martensite volume fraction in the sample was 0.268. A gradual decrease in the content of the α′-martensite phase was observed with increasing polishing time. After 13 h of polishing the same sample, the volume fraction of α′-martensite decreased significantly to 0.002. The initial polishing was carried out by directly "polishing" the sample prepared by Mecut for 50 min. During the initial polishing process, a large amount of deformation-induced α′-martensite was removed, and the α′-martensite volume fraction decreased from 0.268 after mechanical cutting to 0.094, which was caused by the removal of the surface layer with high α′-martensite volume fraction. As the polishing time gradually increased to 115 min and 260 min, the volume fraction of α′-martensite further decreased to 0.078 and 0.049, which indicates that the α′-martensite phase on the surface was continuously removed with further polishing.

To further explore the effect of fine polishing on the removal of surface α′-martensite phase, the polishing time was extended to 6.5 h. Surprisingly, the volume fraction of α′-martensite rebounded to 0.165. This is because the coarser polishing paste (especially the 9 μm one) may introduce a certain amount of new martensitic phase transformation. In the previous steps, due to a residual thickness of high α′-martensite content phase transformation layer from Mecut, polishing using the coarser polishing paste primarily serves to remove/reduce the martensitic transformation layer, hence the reduced α′-martensite content from lab XRD. However, later in the polishing process, as this layer gets thinner, polishing using the coarser polishing paste starts to introduce new DIMT, thus the increased α′-martensite fraction from lab XRD. To examine whether the α′-martensite introduced during polishing at 6.5 h could be subsequently reduced/removed, the polishing protocol was refined by progressively increasing the use of finer abrasives from this point onward. At a total polishing time of 8 h, the α′-martensite volume fraction sharply declined to 0.048, indicating that fine polishing was effective in removing the newly formed α′-martensite induced by previous coarser steps. Subsequent additional polishing using 0.02 μm suspension for 1 h, with a total polishing time of 9 h, further reduced the α′-martensite content to 0.032, suggesting continued elimination of residual surface α′-martensite. To investigate whether prolonged ultra-fine polishing could further reduce the martensitic, polishing was extended to 11 h by incorporating a 0.05 μm suspension for 45 min followed by 0.02 μm suspension for 75 min. However, the volume fraction remained 0.032, suggesting that polishing using the 0.05 μm suspension may have introduced additional α′-martensite and then the 0.02 μm polishing step reduced the α′-martensite content back to the initial value.

Finally, an additional 2 h of polishing with 0.02 μm suspension was conducted, reaching a total duration of 13 h. This led to a further reduction in α′-martensite volume fraction to 0.020, the lowest value observed in this study, suggesting near-complete removal of deformation-induced α′-martensite within the XRD penetration depth. It is possible that this residual fraction represents a lower practical limit of deformation-induced α′-martensite that can exist at room temperature,

Table 4
Specific polishing procedures and α′-martensite volume fractions obtained from XRD for 304 L SS after mechanical cutting, followed by different polishing treatments, with the uncertainties shown representing one standard deviation based on model refinement. Every polishing step in on the top of previous steps.

Sample condition (total polishing time)	Polishing process (time increased from the previous step)	α′-martensitic volume fraction
304 L Mecut	—	0.268 ± 0.003
304 L Mecut + 50 min Polish	9 μm 35 min, 3μm 10 min, 1 μm 5 min	0.094 ± 0.002
304 L Mecut + 115 min Polish	9 μm 40 min, 3 μm 10 min, 1 μm 15 min	0.078 ± 0.003
304 L Mecut + 260 min Polish	9 μm 70 min, 3 μm 15 min, 1 μm 15 min, 0.1 μm 45 min	0.049 ± 0.006
304 L Mecut + 6.5 h Polish	9 μm 90 min, 3 μm 20 min, 1 μm 20 min	0.165 ± 0.002
304 L Mecut + 8 h Polish	1 μm 30 min, 0.1 μm 30 min, 0.02 μm 30 min	0.048 ± 0.004
304 L Mecut + 9 h Polish	0.02 μm 60 min	0.032 ± 0.003
304 L Mecut + 11 h Polish	0.05 μm 45 min, 0.02 μm 75 min	0.032 ± 0.004
304 L Mecut + 13 h Polish	0.02 μm 120 min	0.020 ± 0.003

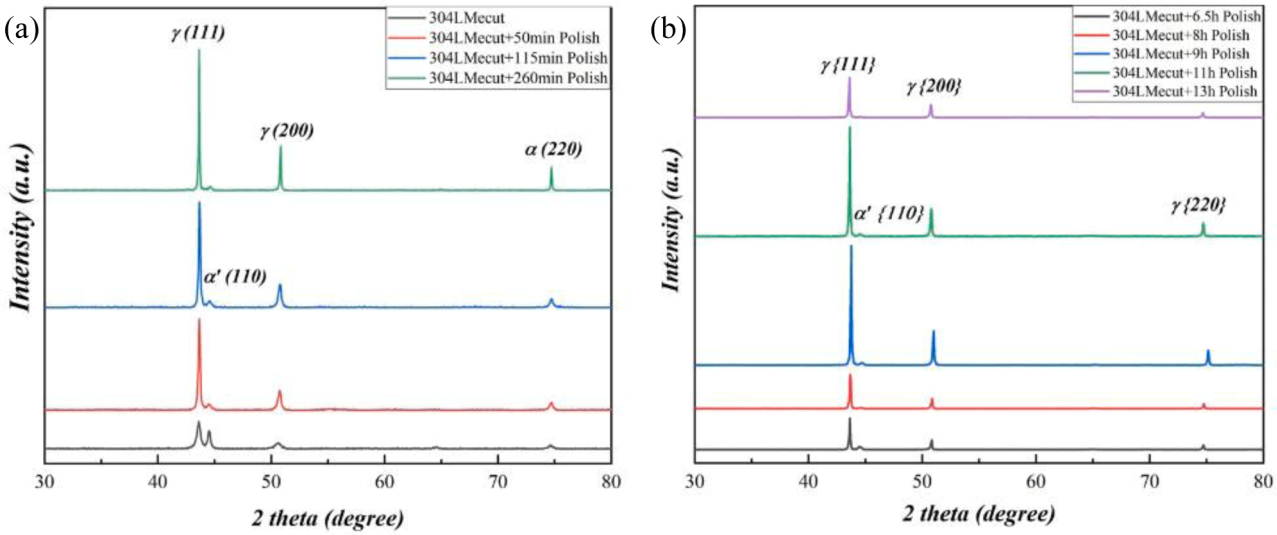

Fig. 7. XRD patterns (collected using Cu Kα radiation) of 304 L SS sample subjected to mechanical cutting (Mecut) followed by polishing: (a) sample cut at 315 rad/s (3000 rpm), feed rate 5.08 mm (0.20 in) /min, with good cooling conditions, and polished on the same surface for 50 min to 260 min; (b) the same sample polished for 6–13 h. All the consecutive steps of sample preparation were performed on the same sample.

arising from unavoidable residual stress and localized strain retained near the surface after polishing, rather than an absolute thermodynamic minimum. Although the deformation-induced α′-martensite was not completely eliminated, its volume fraction was significantly reduced after the final polishing steps. Therefore, when mechanical polishing is employed in the preparation of metastable austenitic SS, it is recommended to appropriately extend the final polishing duration according to the material characteristics and polishing condition, in order to minimize the influence of the sample preparation process on microstructural characterization that might lead to inappropriate interpretation of experimental results and incorrect derivation of the associated mechanisms.

4. Conclusions and remarks

In this study, deformation-induced martensitic transformation (DIMT) in 304 L SS during both room-temperature EDM and mechanical cutting was systematically investigated. The potential impact of surface preparation processes, including grinding and polishing, on the α′-martensite formation was also explored. The key findings can be summarized as follows:

Common sample preparation methods, including mechanical cutting, EDM, and grinding, can induce α′-martensite in metastable 304 L stainless steel and thereby alter the near-surface microstructure that is subsequently interrogated by different characterization techniques. Depending on the preparation route and processing conditions, the measured α′-martensite fraction ranged from nearly undetectable levels to approximately 0.453.

The formation of preparation-induced α′-martensite is governed by the interplay between deformation and temperature. While increased deformation generally promotes martensitic transformation, temperature rises generated during cutting can suppress the γ→α′ transformation, demonstrating that thermal effects may outweigh the influence of strain under certain conditions.

Synchrotron high-energy X-ray diffraction revealed that the transformation is primarily confined to a near-surface layer rather than occurring throughout the bulk material. Consequently, preparation-induced martensite may introduce significant bias into surface-sensitive characterization methods even when the bulk microstructure remains largely unchanged.

Grinding can further increase the amount of preparation-induced martensite through severe surface deformation, highlighting that routine metallographic preparation steps may substantially modify the surface phase constitution and influence subsequent microstructural analysis.

Fine and prolonged polishing effectively removes most of the transformed surface layer, reducing the measured α′-martensite fraction to near-background levels (~0.020). Appropriate polishing procedures are therefore essential for minimizing preparation-induced artifacts and ensuring reliable characterization of metastable austenitic stainless steels.

In many existing studies, the martensitic transformation introduced by surface treatment during sample preparation has been ignored, which may lead to misinterpretation of the final test results. Although consistent cutting and polishing parameters can help mitigate this effect, the significant amount of martensite generated on the surface during preparation may obscure the actual impact of thermal or irradiation effects on phase transformation. This study fills the gap in the current literature on the systematic quantitative research of martensitic transformation induced during sample preparation and provides an important reference for the accuracy of related surface characterization experiments. Although fine polishing can effectively reduce the martensite content, it is still challenging to completely remove the surface transformation, especially when a new DIMT layer is introduced during the coarser polishing stage. While this study primarily focuses on 304 L SS, its findings are expected to be broadly generalizable to a wide range of metastable austenitic steels (i.e., 300 series SS). However, the optimum sample preparation procedures should be adjusted according to the specific alloy composition, initial grain size and other factors.

Future studies may integrate depth-resolved techniques, such as cross-sectional EBSD, to clarify the thickness-dependent distribution of martensitic transformation. In addition, developing standardized sample preparation protocols for metastable austenitic SS, for instance, ensuring the processing temperature remains above the Md temperature, will enhance both microstructural stability and experimental reproducibility.

CRediT authorship contribution statement

Xingshuo Zhang: Writing – review & editing, Writing – original draft, Visualization, Validation, Project administration, Investigation, Formal analysis, Data curation, Conceptualization. **Anish Ranjan:** Writing – review & editing, Formal analysis. **Matthew Luebbe:** Writing – review & editing, Resources, Investigation. **Fan Zhang:** Writing – review & editing, Resources. **Haiming Wen:** Writing – review & editing, Supervision, Resources, Funding acquisition.

Declaration of competing interest

The authors declare that they have no known competing financial interests or personal relationships that could have appeared to influence the work reported in this paper.

Acknowledgements

H.M. Wen would like to thank the U.S. National Science Foundation for financial support (award number DMR-2207965). Materials Research Center at Missouri University of Science and Technology is acknowledged for providing access to characterization equipment. This research used resources of the Advanced Photon Source, a U.S. Department of Energy (DOE) Office of Science User Facility operated for the DOE Office of Science by Argonne National Laboratory under Contract No DE-AC02-06CH11357.

References

[1] M.J. Sohrabi, M. Naghizadeh, H. Mirzadeh, Deformation-induced martensite in austenitic stainless steels: a review, Arch. Civ. Mech. Eng. 20 (2020), https://doi.org/10.1007/s43452-020-00130-1.
[2] P.J. Maziasz, J.T. Busby, Properties of austenitic steels for nuclear reactor applications, Compr. Nucl. Mater. (2012) 267–283.
[3] U. Ehrnstén, P.L. Andresen, Z. Que, A review of stress corrosion cracking of austenitic stainless steels in PWR primary water, J. Nucl. Mater. 588 (2024) 154815, https://doi.org/10.1016/j.jnucmat.2023.154815.
[4] A. Hoffman, M. Arivu, H. Wen, L. He, K. Sridharan, X. Wang, W. Xiong, X. Liu, L. He, Y. Wu, Enhanced resistance to irradiation induced ferritic transformation in nanostructured austenitic steels, Materialia (2020) 100806, https://doi.org/10.1016/j.mtla.2020.100806.
[5] D.L. Porter, Ferrite formation in neutron-irradiated type 304L stainless steel, J. Nucl. Mater. 79 (1979) 406–411.
[6] J.R. Michael, L.A. Giannuzzi, M.G. Burke, X.L. Zhong, Mechanism of FIB-induced phase transformation in austenitic steel, Microsc. Microanal. 28 (2022) 70–82, https://doi.org/10.1017/S1431927621013738.
[7] D.L. Porter, E.L. Wood, In-reactor precipitation and ferritic transformation in neutron-irradiated stainless steels, 1979.
[8] D. Kaoumi, J. Liu, Deformation induced martensitic transformation in 304 austenitic stainless steel: in-situ vs. ex-situ transmission electron microscopy characterization, Mater. Sci. Eng. A 715 (2018) 73–82, https://doi.org/10.1016/j.msea.2017.12.036.
[9] G. Egels, M. Bussmann, S. Benito, S. Weber, On the temperature-dependence of deformation-induced martensite formation in AISI 304L type steel, Metall. Mater. Trans. A Phys. Metall. Mater. Sci. 54 (2023) 4222–4232, https://doi.org/10.1007/s11661-023-07175-w.
[10] David A. Porter, Kenneth E. Easterling, Phase Transformations in Metals and Alloys, Boca Raton, 2009.
[11] A. Rozas, F. Rumiche, J. Sakihama, R. Nuñez, Effect of temperature and speed on the formation of strain-induced martensite in AISI 304L and 316L stainless steels subjected to standardized tensile tests, Metall. Mater. Trans. A Phys. Metall. Mater. Sci. 57 (2026) 1121–1133, https://doi.org/10.1007/s11661-025-08095-7.

[12] G. Egels, M. Bussmann, S. Benito, S. Weber, On the temperature-dependence of deformation-induced martensite formation in AISI 304L type steel, Metall. Mater. Trans. A Phys. Metall. Mater. Sci. 54 (2023) 4222–4232, https://doi.org/10.1007/s11661-023-07175-w.
[13] A. Das, S. Sivaprasad, M. Ghosh, P.C. Chakraborti, S. Tarafder, Morphologies and characteristics of deformation induced martensite during tensile deformation of 304 LN stainless steel, Mater. Sci. Eng. A 486 (2008) 283–286, https://doi.org/10.1016/j.msea.2007.09.005.
[14] H.K. Yeddu, T. Lookman, A. Saxena, Strain-induced martensitic transformation in stainless steels: a three-dimensional phase-field study, Acta Mater. 61 (2013) 6972–6982, https://doi.org/10.1016/j.actamat.2013.08.011.
[15] G. Cios, T. Tokarski, A. Żywczak, R. Dziurka, M. Stępień, M.M. Gondek, B. Pawłowski, K. Wieczerzak, P. Bała, The investigation of strain-induced martensite reverse transformation in AISI 304 austenitic stainless steel, Metall. Mater. Trans. A Phys. Metall. Mater. Sci 48 (2017) 4999–5008, https://doi.org/10.1007/s11661-017-4228-1.
[16] K. Spencer, J.D. Embury, K.T. Conlon, M. Véron, Y. Bréchet, Strengthening via the formation of strain-induced martensite in stainless steels, Mater. Sci. Eng. A 387-389 (2004) 873–881, https://doi.org/10.1016/j.msea.2003.11.084.
[17] J. Liu, D. Kaoumi, Use of in-situ TEM to characterize the deformation-induced martensitic transformation in 304 stainless steel at cryogenic temperature, Mater. Charact. 136 (2018) 331–336, https://doi.org/10.1016/j.matchar.2017.12.005.
[18] J.A. Lichtenfeld, M.C. Mataya, C.J. Van Tyne, Effect of strain rate on stress-strain behavior of alloy 309 and 304l austenitic stainless steel, Metall. Mater. Trans. A. 37 (2006) 147–161, https://doi.org/10.1007/s11661-006-0160-5.
[19] J. Talonen, H. Hänninen, P. Nenonen, G. Pape, Effect of strain rate on the strain-induced $\gamma \rightarrow \alpha'$-martensite transformation and mechanical properties of austenitic stainless steels, Metall. Mater. Trans. A 36 (2005) 421–432, https://doi.org/10.1007/s11661-005-0313-y.J.
[20] S.S. Hecker, M.G. Stout, K.P. Staudhammer, J.L. Smith, Effects of strain state and strain rate on deformation-induced transformation in 304 stainless steel part I. Magnetic measurements and mechanical behavior, 1982. doi:10.1007/BF02644427.
[21] M. Odnobokova, P. Dolzhenko, N. Enikeev, R.Z. Valiev, R. Kaibyshev, A. Belyakov, On the low temperature deformation behavior of a warm rolled 304L-type stainless steel, Materialia (2025) 102372, https://doi.org/10.1016/j.mtla.2025.102372.
[22] J. Burja, J. Lindič, B. Šetina Batič, A. Nagode, Temperature-dependent martensitic transformation in cold-rolled AISI 304 stainless steel, Crystals (2025) 652, https://doi.org/10.3390/cryst15070652.
[23] J. Talonen, H. Hänninen, Formation of shear bands and strain-induced martensite during plastic deformation of metastable austenitic stainless steels, Acta Mater. 55 (2007) 6108–6118, https://doi.org/10.1016/j.actamat.2007.07.015.
[24] F. Peng, X.-H. Dong, K. Liu, H.-Y. Xie, Effects of strain rate and plastic work on martensitic transformation kinetics of austenitic stainless steel 304 ScienceDirect Effects of strain rate and plastic work on martensitic, Transform. Kinet. Austenitic Stainl. Steel. 304 (2014).
[25] W. Zhang, X. Wang, Y. Hu, S. Wang, Predictive modelling of microstructure changes, micro-hardness and residual stress in machining of 304 austenitic stainless steel, Int. J. Mach. Tools Manuf. 130-131 (2018) 36–48, https://doi.org/10.1016/j.ijmachtools.2018.03.008.
[26] L.V. Fricke, G. Gerstein, A. Kotzbauer, B. Breidenstein, S. Barton, H.J. Maier, High strain rate and stress-State-dependent martensite transformation in AISI 304 at low temperatures, Metal (2022) 747, https://doi.org/10.3390/met12050747.
[27] H. Gwon, J. Chae, C. Jeong, H. Lee, D.H. Kim, S.Y. Anaman, D. Jeong, H.H. Cho, Y. K. Kwon, S.J. Kim, H.N. Han, Martensitic transformation during electrochemical polishing of metastable austenitic stainless steel, Acta Mater. 245 (2023) 118612, https://doi.org/10.1016/j.actamat.2022.118612.
[28] A. Hoffman, H. Wen, R. Islamgaliev, R. Valiev, High-pressure torsion assisted segregation and precipitation in a Fe-18Cr-8Ni austenitic stainless steel, Mater. Lett. 243 (2019) 116–119, https://doi.org/10.1016/j.matlet.2019.02.030.
[29] G. Lindwall, C.E. Campbell, E.A. Lass, F. Zhang, M.R. Stoudt, A.J. Allen, L. E. Levine, Simulation of TTT curves for additively manufactured Inconel 625, Metall. Mater. Trans. A Phys. Metall. Mater. Sci 50 (2019) 457–467, https://doi.org/10.1007/s11661-018-4959-7.
[30] F. Zhang, M.R. Stoudt, S. Hammadi, C.E. Campbell, E.A. Lass, M.E. Williams, How austenitic is a martensitic steel produced by laser powder bed fusion? A cautionary tale, Metals 11 (2021) 1924, https://doi.org/10.3390/met11121924.
[31] G.B. Olson, M. Cohen, Kinetics of nucleation strain-induced martensitic, 2009. doi:10.1016/j.mser.2009.03.001.
[32] K. Zhang, K. Wang, Z. Liu, X. Xu, Strain rate of metal deformation in the machining process from a fluid flow perspective, Appl. Sci. 10 (2020) 3057, https://doi.org/10.3390/app10093057.
[33] B. Cao, T. Iwamoto, P.P. Bhattacharjee, An experimental study on strain-induced martensitic transformation behavior in SUS304 austenitic stainless steel during higher strain rate deformation by continuous evaluation of relative magnetic permeability, Mater. Sci. Eng. A 774 (2020) 138927, https://doi.org/10.1016/j.msea.2020.138927.
[34] J. Wang, X. Liu, Z. Ai, G. Dong, M. Huang, C. Shen, Z. Zhang, X. Xi, New insights on the effect of grain size on martensitic transformation in metastable austenite steel, Metall. Mater. Trans. A Phys. Metall. Mater. Sci. 56 (2025) 3355–3365, https://doi.org/10.1007/S11661-025-07839-9.
[35] B. Denkena, B. Breidenstein, M.A. Dittrich, H.N. Nguyen, L.V. Fricke, H.J. Maier, D. Zaremba, Effects on the deformation-induced martensitic transformation in AISI 304 in external longitudinal turning, Adv. Indu. Manuf. Eng. 2 (2021) 100044, https://doi.org/10.1016/j.aime.2021.100044.
[36] G.B. Olson, M. Cohen, Kinetics of strain-induced martensitic nucleation, Metall. Trans. A 6 (1975) 791–795, https://doi.org/10.1007/BF02672301.
[37] A. Dumay, J.P. Chateau, S. Allain, S. Migot, O. Bouaziz, Influence of addition elements on the stacking-fault energy and mechanical properties of an austenitic Fe-Mn-C steel, Mater. Sci. Eng. A 483-484 (2008) 184–187, https://doi.org/10.1016/j.msea.2006.12.170.
[38] S. Allain, J.P. Chateau, O. Bouaziz, S. Migot, N. Guelton, Correlations between the calculated stacking fault energy and the plasticity mechanisms in Fe-Mn-C alloys, Mater. Sci. Eng. A 387-389 (2004) 158–162, https://doi.org/10.1016/j.msea.2004.01.059.
[39] P.C.J. Gallagher, The influence of alloying, temperature, and related effects on the stacking fault energy, Metall. Trans. 1 (1970) 2429–2461, https://doi.org/10.1007/BF03038370.
[40] K.H. Ho, S.T. Newman, State of the art electrical discharge machining (EDM), Int. J. Mach. Tools Manuf. 43 (2003) 1287–1300, https://doi.org/10.1016/S0890-6955(03)00162-7.
[41] Y.C. Lin, B.H. Yan, F.Y. Huang, Surface Improvement Using a Combination of Electrical Discharge Machining with Ball Burnish Machining Based On the Taguchi Method, Springer-Verlag London Limited, 2001.
[42] J. Tang, X. Yang, Simulation investigation of thermal phase transformation and residual stress in single pulse EDM of Ti-6Al-4V, J. Phys. D Appl. Phys. 51 (2018) 135308, https://doi.org/10.1088/1361-6463/aab1a8.
[43] F. Ghanem, C. Braham, H. Sidhom, Influence of steel type on electrical discharge machined surface integrity, J. Mater. Process. Technol. 142 (2003) 163–173, https://doi.org/10.1016/S0924-0136(03)00572-7.
[44] D. Garai, A. Wilson, I. Carlomagno, C. Meneghini, F. Carla, H. Hussain, A. Gupta, J. Zegenhagen, Structure of the surface region of stainless steel: bulk and thin films, Phys. Status Solidi B Basic Res. 259 (2022), https://doi.org/10.1002/pssb.202100513.
[45] M.Y. Al-Shorman, T.C. Jensen, J.N. Gray, High-energy x-ray diffractometer for nondestructive strain depth profile measurement, Rev. Sci. Instrum. 84 (2013), https://doi.org/10.1063/1.4841895.